Vertical profiles of black carbon and nanoparticles pollutants measured by a tethered balloon in an urban settlement in the Arctic

David Cappelletti[a,i*] Chiara Petroselli[b], David Mateos[c], Marcos Herreras[c], Luca Ferrero[d], Asta Gregorič[e], Claudia Frangipani[a,i], Gianandrea La Porta[a], Michael Lonardi[f], Alena Dekhtyareva[g,h]

[a]TRACES Lab, Department of Chemistry, Biology and Biotechnology, University of Perugia, Perugia, Italy;

[b]Faculty of Engineering and Physical Sciences, University of Southampton, University Road, SO17 1BJ, Southampton, UK;

[c]Atmospheric Optics group, Department of Theoretical Physics, Atomic and Optics, University of Valladolid, Valladolid, Spain; ORCID ID: 0000-0001-5540-4721

[d]GEMMA center, Department of Environment and Earth Sciences, The University of Milano-Bicocca, Milan, Italy;

[e]Department of Research & Development, Aerosol d.o.o., Ljubljana, Slovenia;

[f]Leipzig Institute for Meteorology, Lipzig, Germany,

[g]Department of Engineering and Safety, Faculty of Engineering and Technology, UiT The Arctic University of Norway, Tromsø, Norway, ORCID iD;

[h]Geophysical Institute, University of Bergen, and Bjerknes Centre for Climate Research, Bergen, Norway, ORCID iD 0000-0003-4162-7427,

[i]ISP-CNR, Istituto di Scienze Polari, del Consiglio Nazionale delle Ricerche, Bologna, Italy

Abstract

Longyearbyen (Spitsbergen) is a moderately polluted Arctic settlement with the major commercial harbour in the Svalbard islands. Airborne meteorological and aerosol measurements have been performed in Longyearbyen in summer 2018, coupling an instrumental aerosol payload with a meteorological radiosonde deployed on a tethered balloon. More than 70 vertical profiles of aerosol and meteorological properties have been recorded up to a maximum altitude of 1.2 km. As a main result, the present work provides a homogeneous gridded dataset of vertical profiles of equivalent black carbon (*eBC*) and nanoparticle (*NP*) concentrations and associated meteorological data, to be employed for future modelling studies of Arctic pollution. Mean values (± SD) of *eBC* and *NP* below 500 m were 110±10 ng m^{-3} and 1400±400 particles cm^{-3}, respectively. Mean values above 500 m were 150±30 ng m^{-3} and 1000±350 particles cm^{-3}, respectively. The dataset has been complemented by continuous ground measurements of *eBC,* which recorded an average value of 210±130 ng m^{-3} for the entire campaign, with a background value estimated below 100 ng m^{-3} and maximum values in the 1000-2000 ng m^{-3} range. Together with aerosol optical depth measurements, these data allowed for a preliminary discussion of two case studies related to high pollutants concentration events.

1. Introduction

Atmospheric pollution in the Arctic region is a topic of recent and great interest [1] as the Arctic is subject to an amplification of the global warming, with observed temperature increasing almost twice with respect to the global average [2], [3]. Typically, many contaminants are transported towards high latitudes, travelling over long distances in the atmosphere [4]. On the other side, recent anthropization of many Arctic regions poses the question of local, anthropogenic sources of pollutants [5], [6]. These emission sources that include biomass combustion, oil and gas flaring, marine and terrestrial transportation [7] may generate secondary pollutants such as ozone and nitrogen oxides, and hydrocarbons, including volatile organic compounds, carbon monoxide and methane, or aerosols such as black carbon or sulphate aerosols, typically in the nanoparticles size range. Locally emitted pollutants may be dispersed in the atmosphere with different efficiency; therefore, the knowledge of their vertical distribution is of great relevance to assess the local impacts on population and the more general impacts on the Arctic region. In fact, as a general rule, the same type of aerosol can produce different climatic effects and local feedbacks depending on its vertical location [2], [3], [8], [9]. The vertical distribution of aerosol pollutants in the Arctic atmosphere is due to temperature stratification and transport of layered pollution, indicating the influence of different sources at different altitudes [10]. Long-range transported aerosols tend to show higher concentrations in elevated air masses, while emerging anthropogenic sources within the Arctic have been causing intense summer plumes confined in the boundary layers and in proximity of the emission hotspot [11].

The present work reports the results of an intensive summertime experimental campaign realized in Longyearbyen, the major urban settlement in Svalbard Islands. Specifically, daily tethered balloon soundings have been performed in July and August 2018 to investigate vertical aerosol dispersion over Longyearbyen and provide to the scientific community a homogenized dataset of vertical aerosol profiles for further investigations in the coupled modelling-measurements studies. The atmospheric pollutants target of this work are equivalent black carbon (*eBC*) and nanoparticle (*NP*) concentration due to their importance and emission from Longyearbyen as detailed here below.

Experimental studies of *eBC* and *NP* vertical distribution in the Arctic atmosphere are scarce and with inhomogeneous spatial and temporal coverages, if compared with the number of available data collected at ground level [12]. Remote sensing observations, both satellite and ground based, indicate that the highest aerosol concentration in all sectors of the High Arctic and all seasons is observed in the lowest kilometre of the atmosphere [13], [14]. The efficiency of long-range transport of anthropogenic pollutants to Svalbard depends on the position of the Arctic front. In winter and spring, the front shifts southwards and allows for more frequent transport of air masses from mid-latitudes to the Arctic [10], while in summer the front shifts northwards, and the relative importance of local anthropogenic emission sources and their contribution to the total pollution load may increase. Thus, the seasonal peak of aerosol concentration changes as a function of altitude, indicating the influence of different sources and transport at different altitudes [13][15]. If remote sensing observations are fundamental tools to monitor the vertical variability of atmospheric aerosol on large spatial and long temporal scale, in-situ airborne aerosol observations can provide insights on aerosol physics and chemistry. Validation of remote sensing (lidar) data with in-situ (tethered balloons) experiments has been recently proposed [16]. During the Arctic haze period, black carbon concentration tends to increase with altitude already within the first kilometre [17], [18] showing a gradual increase at mid altitudes. In general, lower altitudes were influenced mainly by local Arctic sources, while mid and upper levels were related to transport from eastern Europe, northern and central Asia [19].

2. Experimental methodology

2.1 Tethered balloon launching site

Tethered balloon launches were performed in Longyearbyen (LYB), in the center of Spitsbergen (Figure 1a), specifically from the University Centre in Svalbard (UNIS) CO_2 laboratory located in the valley Adventdalen approximately 5 km to the south-east from Longyearbyen (Fig. 1b) in summer 2018. LYB is the world's northernmost settlement with more than 2000 inhabitants, nowadays is the center of tourism on the archipelago with a notable increase in this activity in the last decades.

a) b)

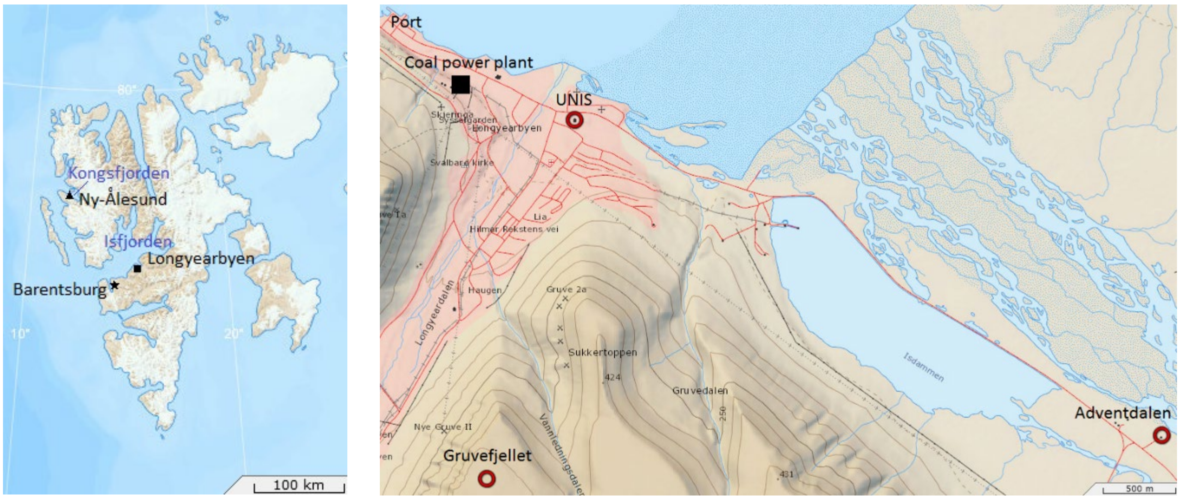

Figure 1. a) Map of Svalbard; b) local map of Longyearbyen (the launching site is marked with the red circle in the Adventalen valley)

The two biggest settlements in Svalbard, Longyearbyen and Barentsburg, are located in Adventfjorden and Grønfjorden, the eastern and southern branches, respectively, of the wide fjord Isfjorden (Fig. 1a). Although stricter regulations to the quality of the ships' fuel used in Svalbard were applied, so that it was restricted to use heavy fuel oil in Kongsfjorden, Isfjorden remained the area where it was still allowed to use oil with maximum sulphur content 3.5%.

The new regulations will prohibit usage of heavy oil in the whole Svalbard territorial waters from January 2022, with exceptions for the traffic of transport ships from and to Longyearbyen and Barentsburg.

Local pollution from ships and the power plant may reach the UNIS CO_2 station only if the wind from the north-west is prevailing; the site has been chosen to not interfere with the aircraft traffic in the area. In fact, all vertical profile measurements have been performed in cooperation with the Svalbard airport (LYB) in the hours when no planes or helicopters were arriving or departing from LYB.

The tethered balloon used to perform vertical profiles (filled with 3.25 m^3 of helium) was used in the hours when ground-based wind speed was below 10 m/s since stronger wind could potentially damage the equipment. In the days when the launch was cancelled due to high wind speed, the wind was in the direction from the Adventdalen valley, therefore, there was no influence of local air pollution from the town on concentrations near the UNIS CO_2 lab. Due to air-traffic and meteorological restrictions, we managed to obtain 78 (39 up and 39 down) vertical meteorological profiles for 52 days of ground-based measurements. 95% of the launches were performed between 12:00 and 18:00 UTC, and only 5% were made from 18:00 to 00:00.

2.2 The aerosol payload

The instrumental payload consisted in a Vaisala meteorological sensors recording *T*, *P* and *RH* data, a micro-aethalometer AE51 for *eBC* data [20] and a MiniDISC portable particle counter for *NP* data [17].

The AE51 microaethalometer (Aethlabs, USA) is a light portable device that records the light attenuation due to the aerosol loaded on a glass-fiber filter at the wavelength of 880 nm. The equivalent black carbon mass concentration (*eBC*) is derived from standard formulas [21] using a mass attenuation cross-section coefficient of 12.5 m^2 g^{-1}, calibrated by the manufacturer. The AE51 was operated with a flux of 200 mL min^{-1} and a time interval of 30 seconds.

The MiniDISC is a miniature diffusion size classifier, a small and portable instrument [22]. This device has a d50 cutoff at 14 nm, therefore, it underestimates particle number concentrations for particles smaller than 20 nm while, above this threshold, acts as a total particle counter. The instrument was operated at 1 second time resolution and the data were post-processed at 10 seconds with the Java routine supplied by the manufacturer.

Both the MiniDISC and AE51 have not been used when the air humidity was too high (relative humidity above 90% was used as a threshold). Moreover, the MiniDISC has been employed for a shorter period of time (6 Jul-11Aug) than the AE51 (3 Jul-15 Aug). In total, 74 equivalent black carbon (eBC) and 52 nanoparticle number (NP) concentration profiles were obtained.

2.3 Vertical profile data post-processing

In order to reduce the noise of concentration data obtained using high time resolutions, post-processing algorithms can be used. This procedure is particularly important for the *eBC* data, which show a high point-to-point variability while *NP* measurements are more stable. The following procedure has been implemented:

1) The rate of pressure and temperature change with time d*P*/d*t* and d*T*/d*t* have been calculated for ascending and descending profiles separately.

2) The calculated rates have been checked for normality of distribution using Kolmogorov-Smirnov test in the Matlab software.

3) Since the data are not normally distributed, a robust measure to detect outliers has been chosen. The outliers in the d*P*/d*t* and d*T*/d*t* data have been defined as all points more than three

scaled median absolute deviation (MAD) from the median values [23].

4) Pressure values for these outlier points are changed to the linearly interpolated value between closest non-outlier pressure points. As the sampling rate is irregular, the interpolation is done considering local time interval between two nearest non-outlier points. This method removes only extreme outliers; it does not smooth the data and the processing result is still close to the original values.

5) The height has been calculated from pressure using hypsometric equation [24], which is common to use for radiosonde profiles.

6) To compare *eBC* (or *NP*) profiles with the meteorological values, the height, temperature and wind speed have been averaged for 30 sec periods according to the timing at AE51 (or *NP*) sensor.

7) *eBC* data smoothing has been performed using 1-2-1 smoothing filter [25]. Even after the smoothing, the AE51 provided few negative values for *eBC*. The proportion of negative values of *eBC* was 11.2 %, considering the raw data at 30 s acquisition time. After the 50 m averages used to grid the dataset (see below) the proportion of negative values reduced to 7.1%. These values are in agreement with other experiments carried out with the AE51 [26].

Both instruments were previously tested and compared with ground-based bench instruments in Ny Alesund [17], [27], providing also an assessment of their accuracy and detection limits.

2.4 Complementary ground-based aerosol measurements and inter-comparison of eBC data

The dataset was complemented with several other measurements within a larger experimental campaign. In particular relevant for the present paper, a seven channels Aethalometer model AE33 (Magee Scientific) was placed in the office on the third floor at UNIS building in LYB, where the inlet of the sampling hose was fixed outside from the window. The data have been accumulated continuously at 1 min time resolution and 5 l/min flow rate for all the field campaign. Meteorological data have also been recorded along the campaign.

The AE51 sensor was inter-compared in-situ at the UNIS site with the ground based AE33 monitor eight times throughout the campaign with an average calibration period of two hours each time. The temperature, humidity and wind speed range during the calibrations were 4.4°C-14.4°C, 60%-100%, 0 $m·s^{-1}$-7.6$m·s^{-1}$, respectively. AE33 data with 1-mine resolution was compared with 1-minute averaged data from AE51. The worst and the best correlation between the two instruments were obtained the 21/07/2018 and the 01/08/2018 when the mean concentration of *eBC* measured by AE33 was the lowest (191 $ng·m^{-3}$) and the highest (1051 $ng·m^{-3}$), respectively. The correlation between the *eBC* values of the two instruments was calculated for the four groups of data (quartiles). Results of intercomparison show improved agreement in the higher concentration range.

The same procedure has been done for quartiles of air temperature, relative humidity and wind speed to check if these values influence the correlation, but no significant difference in correlation coefficients has been found for different groups within the range of meteorological parameters during calibration. The details of the inter-comparison are reported in the Supplementary Material. Since the concentrations of *eBC* measured during soundings in Adventdalen were very low, often within the 1st quartile of AE33 data, high uncertainty in absolute values of *eBC* data measured by AE51 has to be considered. However, since 50m-average values were applied to study profiles' statistics, this averaging eliminated some of the noise. Relative *eBC* concentration profile still carry important information.

3 Results and discussion

3.1 Weather conditions in the study area

Weather conditions in the investigated area (Old Auroral Station; 78°12’08”N, 15°49’42”E) are given by the combination of synoptic circulation and local topography. Winds aloft are typically south-westerly or north-easterly [28]. The investigated period saw several low pressure systems approaching from the south-west and advecting warmer air. The orography of the area, characterized by 500 m high plateaus separated by valleys, controls the flows at lower altitudes [29], with wind channelling occurring in the valleys. The study period covers the transition between the summer solstice and the end of the polar day (3 July-15 August, 2021). The surface energy budget is impacted by large solar irradiances and low albedo.

Local conditions in the valley Adventdalen were derived using hourly data from the local 10 m weather mast. A weather station located at 464 m a.s.l. on the neighbouring plateau Gruvefjellet was used to gain representative data for the upper parts of balloon vertical profiles. The topography surrounding the balloon site typically induced wind channeling along Adventdalen valley (~135° and ~315°), decoupling the lowermost 400-500 m of the Atmospheric Boundary Layer (ABL) from the large scale circulation. A diurnal cycle in winds and temperature in Adventdalen gradually gained importance in August. The wind aloft the plateau was generally southerly or easterly, following the synoptic circulation. The wind inside the valley was typically channelled from Adventfjord towards the station (Fig SM1a). An average wind speed of 3-4 ms^{-1} was measured at the mountain and the valley sites, with intensities never dropping below 1 ms^{-1} (Fig SM1b).

Three periods were particularly influenced by the synoptic activity: (L) 8-13 July, (L) 22-26 July and (H) 2-6 August. During these events, the passage of pressure systems was associated with increased wind speeds and constant wind directions inside and above the valley.

The surface temperature at the Old Auroral Station was 7°C on average, with temperature increasing until early August, when the maximum hourly temperature of 12 °C was recorded (Fig SM1c). Temperature at the mountain site was generally lower due to the height difference. Humidity was systematically above 60% (Fig SM1d), with low-level clouds forming above the valley.

3.2 Construction of gridded vertical profiles

The pre-processed vertical profiles of *eBC* and *NP* are reported in Figure 2.

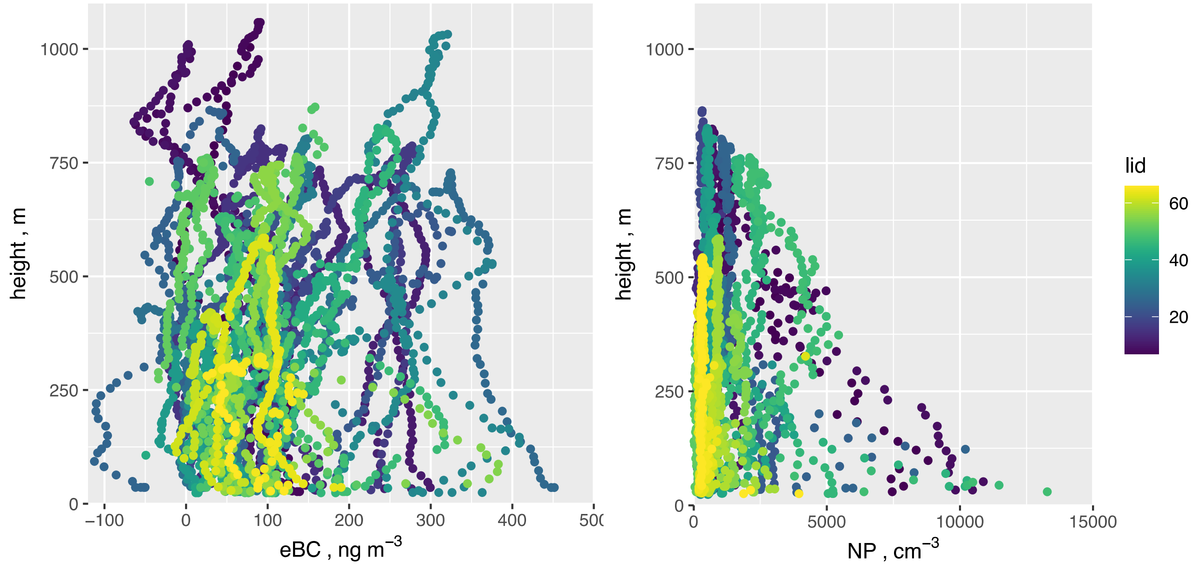

Figure 2 – Ungridded vertical profiles of (a) *eBC* and (b) *NP*. The colour scale identifies the launch id (lid).

Most of the profiles have been obtained in the first 750 m and only six launches reached the elevation of 1 km. *eBC* profiles showed a larger variability both in magnitude and in vertical trend as compared to the *NP* profiles.

The gridded vertical profile datasets have been constructed by averaging the pre-processed data accumulated in 50 m vertical bins and assigned to the middle of the vertical bin (for example: the first point has been generated at 25 m above ground, including data from 0 to 50 m). Data points in each vertical bin ranged from two to ten. The gridded profiles are presented in Figure 3.

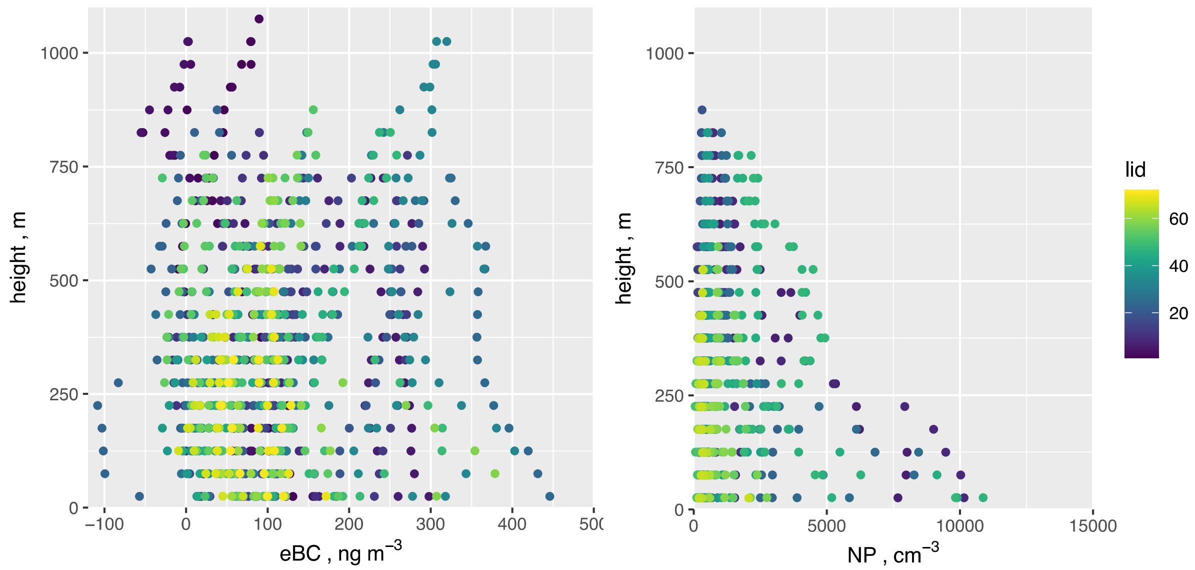

Figure 3 – Gridded vertical profiles of (a) *eBC* and (b) *NP*. The colour scale identifies the launch id (lid).

Temperature (T), relative humidity (RH), pressure (P) and wind speed (ws) have also been gridded on the same 50 m vertical scale. This allowed to study the general phenomenology and to produce seasonally averaged profiles on a homogeneous vertical grid.

3.3 Vertical profiles: general phenomenology

The maximum height of 33% of Adventdalen profiles was less than 500 m, 59 % of the profiles were between 500 and 1000 m, and 8 % above 1000 m. For this group, according to WRS-test, median ground-level wind speed was significantly higher than for the rest of the profiles (5.4 m/s vs 4.3 m/s). According to the WRS-test, median profile wind speed and air temperature below 1000 m were significantly higher for the measurements with temperature inversions height, *zTb,* starting below 500 m, than for those with inversion starting above 500 m (shown in bold in Table 1). The opposite relationship was observed for relative humidity in the two groups. Profiles without temperature inversions had the highest median wind speed and lowest median profile temperature (see Table 1).

Synoptic scale meteorological situation for the three groups ((a) without temperature inversions in Adventdalen, (b) with temperature inversions detected below 500 m height and (c) with inversions starting above 500 m) are shown in Figure SM2. Both (a) and (b) group of days were characterized by high-pressure system located to the south-east of Svalbard. However, the south-westerly wind with higher wind speed was prevailing during the (a) group of measurements, while in the (b) group, the wind speed was lower and air masses transported from the south were warmer, since higher air temperatures were over Scandinavia. In the (c) group of days (*zTb*>500m*)*, the north-westerly wind with low wind speed was bringing humid air from North Atlantic to Svalbard. Results of wind measurements for the same three groups from Longyearbyen (24 m a.s.l.), Adventdalen (15 m a.s.l.) and Gruvefjellet (464 m a.s.l.) are shown in Figure SM2 (d, e and f.) The mean wind speed observed in Adventdalen was almost the same for the three groups, however, according to the data from the Gruvefjellet station, the wind speed aloft was lower for the days with temperature inversions. The wind direction in Adventdalen was always north-westerly, along the valley axis, while in the days without temperature inversion, the wind direction observed at Gruvefjellet (Fig. SM2d) was similar to the large scale flow (Fig. SM2a). In most cases, north-westerly and westerly wind direction in Longyearbyen was favourable for transport of local pollutants towards Adventdalen valley, where *eBC* soundings were performed, except a few days when south-westerly flow was observed in the town similarly to the measurements made at the Gruvefjellet station.

The statistics of vertical *eBC* and *NP* concentration measurements for the three groups, is reported in Table 1. There is a positive statistically significant correlation between the height of maximum *eBC* concentrations and height of minimum wind speed in the profiles ($r=0.44$, $p<0.001$). Indeed, in 92% of all profiles, the height of maximum *eBC* concentration is less or equal to the height of minimum wind speed. On average, maximum *eBC* concentrations could be found around 230m below the height of minimum wind speed. The correlation between the height of maximum concentration and the height of the maximum temperature is not statistically significant.

Since the number of profiles with *zTb*>=500m is very small, the groups with *zTb*<500m and *zTb*>=500m have been combined into one group with 31 *eBC* profiles ($n_{BC}=31$) and 16 *NP* profiles ($n_{part}=16$) and compared with a group when no temperature inversions were observed ($n_{BC}=43$, $n_{part}=32$). According to the WRS-test, there is no statistically significant difference between median concentrations for the two groups, while the median concentration of *NP* in the profiles with temperature inversion was significantly higher than in profiles where no inversions were observed ($p<0.001$). Group medians of maximum *eBC* and *NP* concentrations in profiles with temperature inversions were significantly higher. Similarly, median *eBC* concentration measured in Longyearbyen for two hours before the sounding to the time of tethered balloon launch with *eBC* sensor in Adventdalen was higher when temperature inversion was observed (p<0.001?).

Overall, homogeneous profiles (no temperature inversions) have been observed for 60% of the cases for the present summertime 2018 campaign in Longyearbyen, which can be compared with the 40% homogeneous profiles observed in the summertime 2012 in Ny Alesund [30]. The difference could be attributed to the year-to-year variability as well as to the different orography of the launching sites, which may influence the aerosol mixing in the boundary layer.

3.4 An example of use of the gridded dataset: local sources versus long-range transport

The present dataset can be exploited to unveil the relative role of local and long-range sources of pollutants. We discuss here a first simple example to study the influence of local versus remote sources to the *eBC* levels in LYB. The *eBC* general trend is well described by the data from AE33 instruments running in LYB on 1 minute time resolution. A preliminary analysis of this dataset provided background *eBC* values for the summer season in LYB, which were typically lower than 100 ng m^{-3}. The analysis highlighted also the presence of sharp *eBC* peaks lasting from 1 to 10 minutes with *eBC* values in the 1000-2000 ng m^{-3} range, which can be connected to the local pollution sources. The overall average value of *eBC* for the campaign was 208±130 ng m^{-3}. The daily average of the 1 minutes *eBC* values is reported in Figure 3. Even after averaging, the daily values are significantly higher than the background, with a high day-to-day variability. We investigated two case studies: the 1st August during which the highest *eBC* daily value of the season, 780 ng m^{-3}, was reached, and the 13th of August, with a daily average *eBC* of 286 ng m^{-3}.

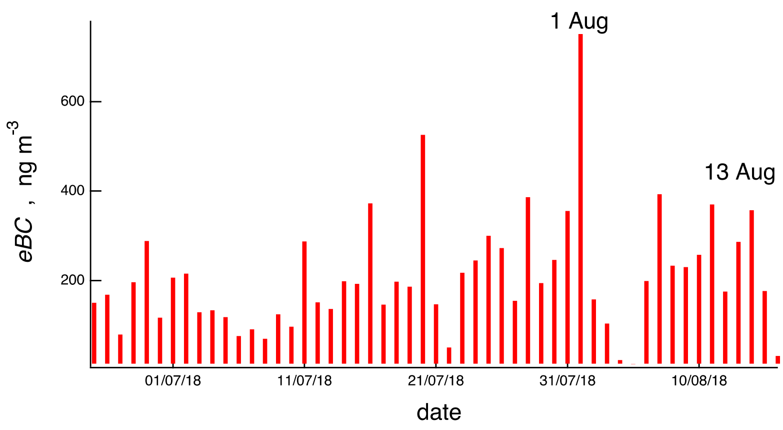

Figure 4 – Daily average eBC measured in LYB by the AE33.

The vertical profiles of eBC, temperature and wind speed, recorded with the tethered balloon system on the 1st of August at 15:00 UTC and on the 13 of August at 16:30 UTC are reported in Figure 5. The profiles on the 1st of August clearly indicate a stratification of *eBC* in the first 200 meters associated with a temperature inversion at approximately 300 m a.s.l. and low wind speed pointing at an apparent influence of local sources. By contrast, a significant layer of *eBC* , up to nearly 600 ng m^{-3}, was present on the 13th of August around 900-1000 meters and associated with a high wind speed layer. The median eBC concentrations measured in profile from soundings in Adventdalen on that day were higher than average (294 ng·m^{-3}). There was no pronounced temperature inversion, probably due to the mixing of the boundary layer due to high wind speed.

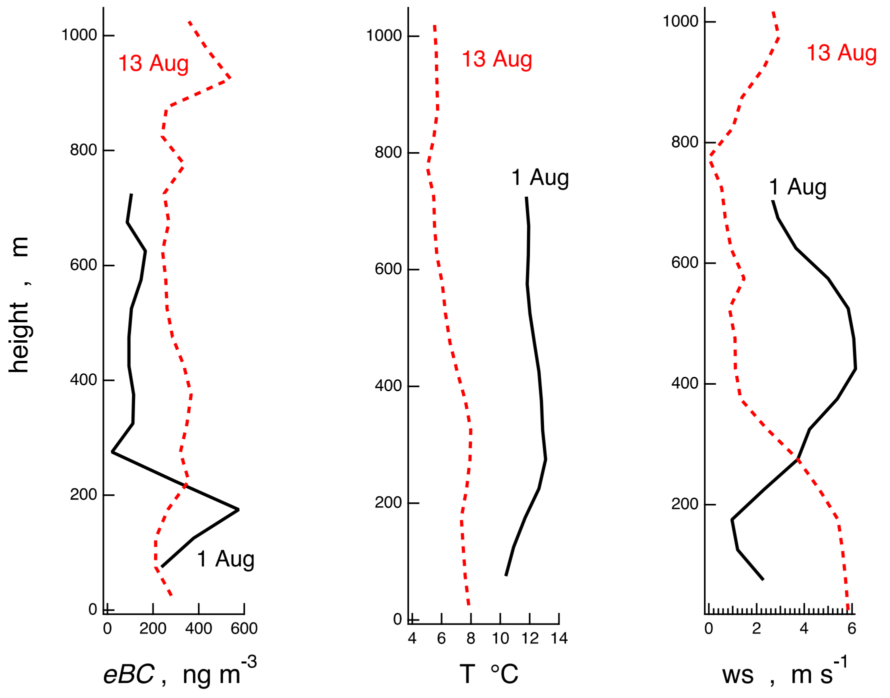

Figure 5 – Vertical profiles of eBC, temperature and wind speed registered with the tethered balloon system on the 1st of August (black continuous lines) and on the 13 of August (red dashed lines).

This aerosol outbreak event extended to the whole Svalbard archipelago and was also identified in the columnar AOD data from Longyearbyen, Ny-Ålesund, and Barentsburg on the 13th of August. The two former sites belong to AERONET (Longyearbyen and Ny_Alesund_AWI sites) and data from version 3 – level 2.0 are presented here. Barentsburg SP-9 sun photometer measures solar irradiance between 300 and 2200 nm which includes GPS, tracker and cloud screening. Figura 6a shows the general situation of Ångström Exponent 440/870 nm as a function of the AOD at 500 nm for the three sites during the campaign. Data from the August 13th are highlighted in stronger colours. Strong AOD values (at 500 nm) between 0.2 and 0.7 are reported in the three sites simultaneously. As recorded in the three sites, there is a sharp increase in AOD values: AOD double its value in less than 4 hours. In spite of the different techniques and methods no particular variation of the Ångström Exponent is observed in the archipelago during the aerosol outbreak. Ångström Exponent values are around 1.5 with a slight decrease up to 1.4, which indicates the predominant presence of small particles in the atmospheric column.

Figure 6b) shows the size distribution inversions for August 13th for Longyearbyen and Ny-Ålesund (AERONET sites). There is a large concentration of particles with radius below 0.4 µm, so that event is dominated by the fine mode particles. The event is becoming stronger with time and no significant differences are obtained between Longyearbyen and Ny-Ålesund (112 km apart).

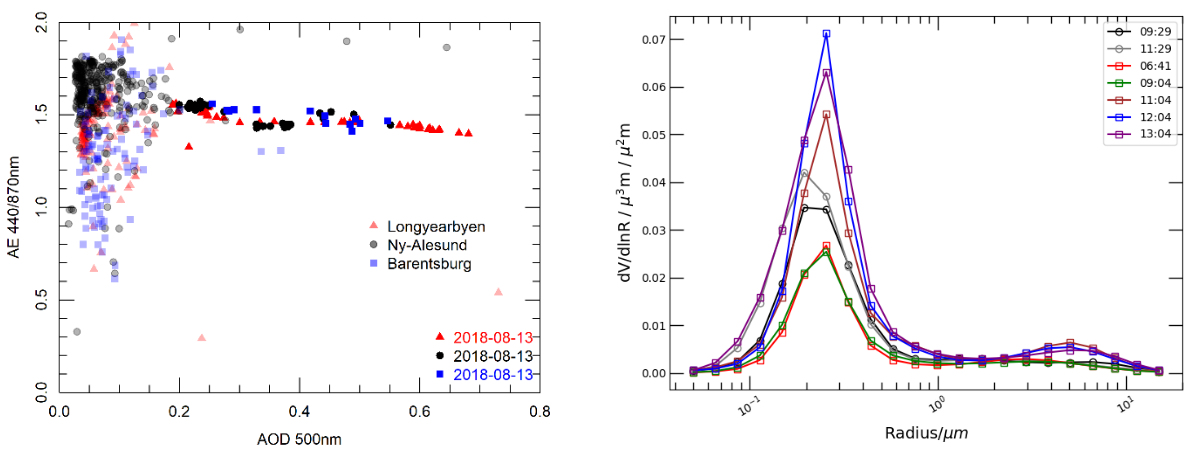

Figure 6 - a) Angstrom Exponent 440/870 nm as a function of the AOD at 500 nm; b) size

distribution inversions for August 13th for Longyearbyen and Ny-Ålesund.

It is noteworthy that on the 13th August, the wind speed and temperature profiles (Figure 5) highlight three atmospheric layers: one from ground till 300 m, one between 300 and 800 m and the last one above it. Thus, the higher *eBC* concentration layer can be considered separated from the bottom one ensuring the non-local origin of its source. According to backward trajectories analyses (HYSPLIT [31]) for the 13th of August, the air masses were arriving from the Northern sectors of Eurasia (see supplementary material), where the probable source of *eBC* is located.

3.5 Averaged vertical profiles

The gridded dataset allowed to calculate averaged vertical profiles of the measured properties which represent a description of the summertime Longyearbyen atmospheric column. Results are shown in Figure 7-8 for *eBC, NP, T, RH* and wind speed, respectively.

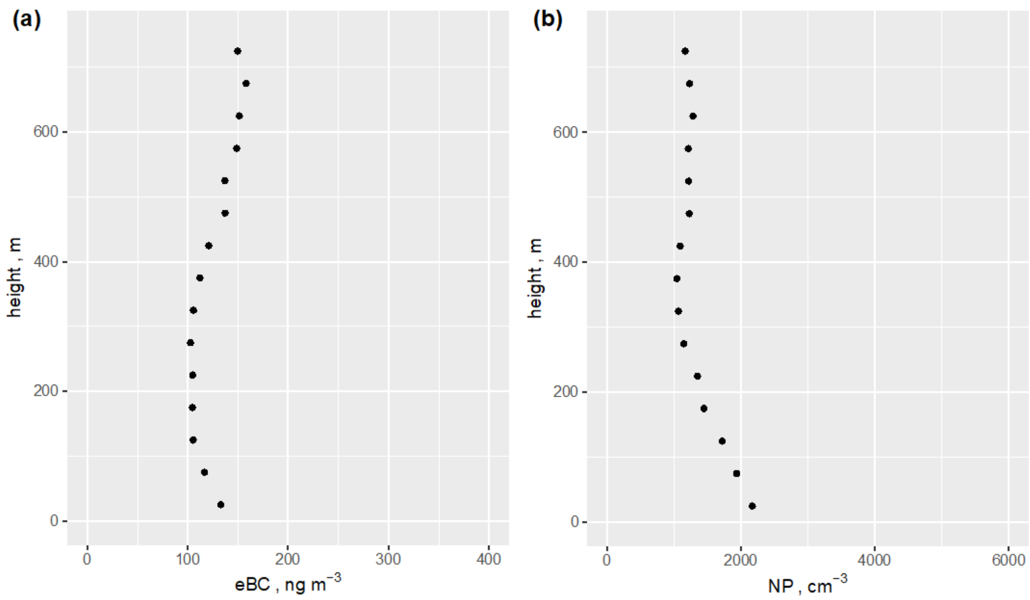

Figure 7 – Summertime averaged *eBC* and *NP* profiles along the atmospheric column over Longyearbyen in 2018. Shaded areas represent the 95% confidence interval of the population.

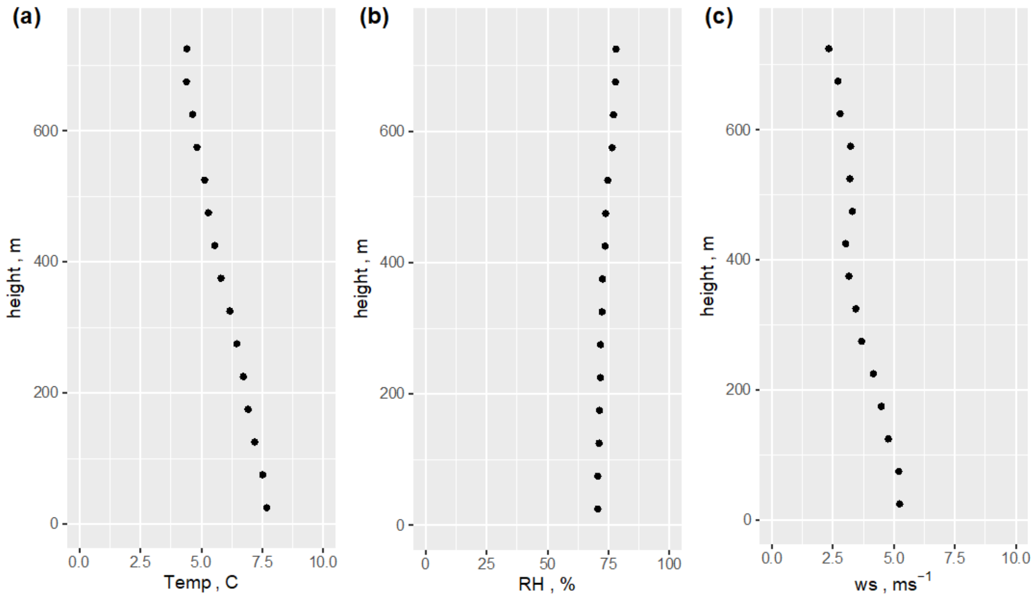

Figure 8 – Summertime averaged *T, RH* and wind speed (*ws*) profiles along the atmospheric column over Longyearbyen in 2018. Shaded areas represent CI95% intervals.

The tethered balloon averaged profiles reported in Figures 7-8 highlight the presence of marked aerosol stratification for nanoparticles close to the ground and a higher level of *eBC* at higher altitude (above 500 m). The *eBC* behaviour was in keeping with a higher wind speed around 500 m. The aforementioned results describe a situation previously observed in late spring over Ny-Ålesund, in which a plume of nanoparticle (probably of secondary origin) is present close to the ground.

In this respect, it has been recently demonstrated that the final vertical aerosol profiles can result from the synergy between the seasonal behaviour of aerosol and the local meteorology [30], [32], [33]. The importance of classifying average aerosol profiles in function of the season and meteorological situation is related to their feedback on climate [12], [17]. An increase of aerosol concentration with altitude can influence the cloud cover (inducing mainly a positive forcing) while aerosol and BC/dust layers located immediately above snow and ice may induce a positive forcing, the opposite of the effect they have when aerosol layer is present at high altitude, especially above clouds.

4. Conclusion

The main goal of the present work is to generate a homogeneous gridded dataset of aerosol vertical profiles recorded in a summertime long campaign in Longyearbyen (Svalbard Islands). Main aerosol properties, such as equivalent black carbon and total particle concentrations, have been measured with a tethered balloon system in the first kilometre of the troposphere above this anthropized Arctic settlement.

Temperature inversions, created by the warm air advection from Scandinavia to Svalbard, promote the conditions favourable for the accumulation of local pollutants in the Arctic boundary layer. However, elevated concentrations may be observed in Longyearbyen even in the absence of the long-range transported pollution. In these days, colder air masses were brought by the large-scale westerly wind. The wind direction changed to north-westerly due to channelling along the Adventdalen valley, and locally polluted air was efficiently transported from the major local emission sources, the coal power plant and ships, to the valley.

The vertical structure of summer ABL in Adventdalen (Longyearbyen) was similar to that of Ny-Ålesund [17], [34], with higher median wind speed and lower air temperatures in the profiles without temperature inversions and higher air temperature and lower wind speed in the profiles with inversions at both sites. In the days with temperature inversions, higher maximum *eBC* concentrations and particle concentrations were observed in Adventdalen profiles and by ground-based measurements in Longyearbyen.

Acknowledgements

Dr. Kim Holmén is gratefully thanked for the invaluable advice on local pollution sources in Ny-Ålesund and Longyearbyen. Research technician Vitaly Dekhtyarev is acknowledged for support with electronic equipment and data processing during the field work in Longyearbyen in 2018. We thank UNIS for providing meteo data. We also acknowledge the AMIS project and the GEMMA center in the framework of the MIUR project "Dipartimenti di Eccellenza 2018-2022".

Funding

The Research Council of Norway financed the pilot study in Longyearbyen. The field work was a part of the project "Strengthening cooperation on air pollution research in Svalbard" received the support via Svalbard Strategic Grant (n. 283475).

References

[1] K. S. Law and A. Stohl, "Arctic air pollution: Origins and impacts," *Science (80-.).*, vol. 315, no. 5818, pp. 1537–1540, 2007, doi: 10.1126/science.1137695.

[2] H. Goosse *et al.*, "Quantifying climate feedbacks in polar regions," *Nat. Commun.*, vol. 9, no. 1, 2018, doi: 10.1038/s41467-018-04173-0.

[3] M. C. Serreze and R. G. Barry, "Processes and impacts of Arctic amplification: A research synthesis," *Glob. Planet. Change*, vol. 77, no. 1–2, pp. 85–96, 2011, doi: 10.1016/j.gloplacha.2011.03.004.

[4] L. A. Barrie *et al.*, "Arctic contaminants: sources, occurrence and pathways," *Sci. Total Environ.*, vol. 122, no. 1–2, pp. 1–74, 1992, doi: 10.1016/0048-9697(92)90245-N.

[5] J. Schmale *et al.*, "Local Arctic Air Pollution: A Neglected but Serious Problem," *Earth's Futur.*, vol. 6, no. 10, pp. 1385–1412, 2018, doi: 10.1029/2018EF000952.

[6] K. S. Law *et al.*, "Local Arctic air pollution: Sources and impacts," *Ambio*, vol. 46, no. s3, pp. 453–463, 2017, doi: 10.1007/s13280-017-0962-2.

[7] A. Roiger *et al.*, "Quantifying emerging local anthropogenic emissions in the arctic region: The access aircraft campaign experiment," *Bull. Am. Meteorol. Soc.*, vol. 96, no. 3, pp. 441–460, 2015, doi: 10.1175/BAMS-D-13-00169.1.

[8] L. Ferrero *et al.*, "Impact of black carbon aerosol over Italian basin valleys: High-resolution measurements along vertical profiles, radiative forcing and heating rate," *Atmos. Chem. Phys.*, vol. 14, no. 18, 2014, doi: 10.5194/acp-14-9641-2014.

[9] T. Su *et al.*, "The significant impact of aerosol vertical structure on lower atmosphere stability and its critical role in aerosol-planetary boundary layer (PBL) interactions," *Atmos. Chem. Phys.*, vol. 20, no. 6, pp. 3713–3724, 2020, doi: 10.5194/acp-20-3713-2020.

[10] M. A. Thomas, A. Devasthale, M. Tjernström, and A. M. L. Ekman, “The Relation Between Aerosol Vertical Distribution and Temperature Inversions in the Arctic in Winter and Spring,” *Geophys. Res. Lett.*, vol. 46, no. 5, pp. 2836–2845, 2019, doi: 10.1029/2018GL081624.

[11] J. A. Mayfield and G. J. Fochesatto, “The layered structure of the winter atmospheric boundary layer in the interior of Alaska,” *J. Appl. Meteorol. Climatol.*, vol. 52, no. 4, pp. 953–973, 2013, doi: 10.1175/JAMC-D-12-01.1.

[12] B. H. Samset *et al.*, “Modelled black carbon radiative forcing and atmospheric lifetime in AeroCom Phase II constrained by aircraft observations,” *Atmos. Chem. Phys.*, vol. 14, no. 22, pp. 12465–12477, 2014, doi: 10.5194/acp-14-12465-2014.

[13] T. Shibata, K. Shiraishi, M. Shiobara, S. Iwasaki, and T. Takano, “Seasonal Variations in High Arctic Free Tropospheric Aerosols Over Ny-Ålesund, Svalbard, Observed by Ground-Based Lidar,” *J. Geophys. Res. Atmos.*, vol. 123, no. 21, pp. 12,353-12,367, 2018, doi: 10.1029/2018JD028973.

[14] A. Devasthale and M. A. Thomas, “A global survey of aerosol-liquid water cloud overlap based on four years of CALIPSO-CALIOP data,” *Atmos. Chem. Phys.*, vol. 11, no. 3, pp. 1143–1154, 2011, doi: 10.5194/acp-11-1143-2011.

[15] S. J. Doherty, T. C. Grenfell, S. Forsström, D. L. Hegg, R. E. Brandt, and S. G. Warren, “Observed vertical redistribution of black carbon and other insoluble light-absorbing particles in melting snow,” *J. Geophys. Res. Atmos.*, vol. 118, no. 11, pp. 5553–5569, 2013, doi: 10.1002/jgrd.50235.

[16] L. Ferrero *et al.*, “Aerosol optical properties in the Arctic: The role of aerosol chemistry and dust composition in a closure experiment between Lidar and tethered balloon vertical profiles,” *Sci. Total Environ.*, vol. 686, 2019, doi: 10.1016/j.scitotenv.2019.05.399.

[17] L. Ferrero *et al.*, "Vertical profiles of aerosol and black carbon in the Arctic : a seasonal phenomenology along 2 years (2011 – 2012) of field campaigns," *Atmos. Chem. Phys.*, vol. 16, pp. 12601–12629, 2016, doi: 10.5194/acp-16-12601-2016.

[18] K. M. Markowicz *et al.*, "Vertical variability of aerosol single-scattering albedo and equivalent black carbon concentration based on in-situ and remote sensing techniques during the iAREA campaigns in Ny-Ålesund," *Atmos. Environ.*, vol. 164, 2017, doi: 10.1016/j.atmosenv.2017.06.014.

[19] H. Schulz *et al.*, "High Arctic aircraft measurements characterising black carbon vertical variability in spring and summer," *Atmos. Chem. Phys.*, vol. 19, no. 4, pp. 2361–2384, 2019, doi: 10.5194/acp-19-2361-2019.

[20] L. Ferrero, G. Mocnik, B. S. Ferrini, M. G. Perrone, G. Sangiorgi, and E. Bolzacchini, "Vertical profiles of aerosol absorption coefficient from micro-Aethalometer data and Mie calculation over Milan," *Sci. Total Environ.*, vol. 409, no. 14, pp. 2824–2837, 2011, doi: 10.1016/j.scitotenv.2011.04.022.

[21] A. D. A. HANSEN, H. ROSEN, and T. NOVAKOV, "The Aethalometer," *Sci. Total Environ.*, vol. 36, pp. 191–196, 1984.

[22] M. Fierz, C. Houle, P. Steigmeier, and H. Burtscher, "Design, Calibration, and Field Performance of a Miniature Diffusion Size Classifier," *Aerosol Sci. Technol.*, vol. 45, no. 1, pp. 1–10, 2011, doi: 10.1080/02786826.2010.516283.

[23] P. J. Rousseeuw and M. Hubert, "Robust statistics for outlier detection," *WIREs Data Min. Knowl. Discov.*, vol. 1, pp. 73–79, 2011, doi: 10.1002/widm.2.

[24] J. M. Wallace and P. V. Hobbs, *Atmospheric science: an introductory survey*, 2nd ed. New York: Academic Press, 2006.

[25] X. Y. Wang and K. C. Wang, "Estimation of atmospheric mixing layer height from radiosonde data," *Atmos. Meas. Tech.*, vol. 7, pp. 1701–1709, 2014, doi: 10.5194/amt-

7-1701-2014.

[26] T. Miyakawa, P. Mordovskoi, and Y. Kanaya, “Evaluation of black carbon mass concentrations using a miniaturized aethalometer: Intercomparison with a continuous soot monitoring system (COSMOS) and a single-particle soot photometer (SP2),” *Aerosol Sci. Technol.*, vol. 54, no. 7, pp. 811–825, 2020, doi: 10.1080/02786826.2020.1724870.

[27] B. Moroni *et al.*, “Vertical Profiles and Chemical Properties of Aerosol Particles upon Ny-Ålesund (Svalbard Islands),” *Adv. Meteorol.*, vol. 2015, 2015, doi: 10.1155/2015/292081.

[28] I. Hanssen-Bauer and E. Førland, “Verification and analysis of a climate simulation of temperature and pressure fields over Norway and Svalbard,” *Clim. Res.*, vol. 16, no. 3, pp. 225–235, 2001, doi: 10.3354/cr016225.

[29] S. Mayer, M. O. Jonassen, A. Sandvik, and J. Reuder, “Profiling the Arctic Stable Boundary Layer in Advent Valley, Svalbard: Measurements and Simulations,” *Boundary-Layer Meteorol.*, vol. 143, no. 3, pp. 507–526, 2012, doi: 10.1007/s10546-012-9709-6.

[30] L. Ferrero *et al.*, “Vertical profiles of aerosol and black carbon in the Arctic: A seasonal phenomenology along 2 years (2011-2012) of field campaigns,” *Atmos. Chem. Phys.*, vol. 16, no. 19, 2016, doi: 10.5194/acp-16-12601-2016.

[31] A. F. Stein, R. R. Draxler, G. D. Rolph, B. J. B. Stunder, M. D. Cohen, and F. Ngan, “Noaa’s hysplit atmospheric transport and dispersion modeling system,” *Bull. Am. Meteorol. Soc.*, vol. 96, no. 12, pp. 2059–2077, 2015, doi: 10.1175/BAMS-D-14-00110.1.

[32] C. A. Brock *et al.*, “Characteristics, sources, and transport of aerosols measured in spring 2008 during the aerosol, radiation, and cloud processes affecting Arctic Climate

(ARCPAC) Project," *Atmos. Chem. Phys.*, vol. 11, no. 6, pp. 2423–2453, 2011, doi: 10.5194/acp-11-2423-2011.

[33] D. J. Jacob *et al.*, "The arctic research of the composition of the troposphere from aircraft and satellites (ARCTAS) mission: Design, execution, and first results," *Atmos. Chem. Phys.*, vol. 10, no. 11, pp. 5191–5212, 2010, doi: 10.5194/acp-10-5191-2010.

[34] B. Moroni *et al.*, "Local vs. long-range sources of aerosol particles upon Ny-Ålesund (Svalbard Islands): mineral chemistry and geochemical records," *Rend. Lincei*, vol. 27, 2016, doi: 10.1007/s12210-016-0533-7.

[35] J. Backman *et al.*, "On Aethalometer measurement uncertainties and an instrument correction factor for the Arctic," *Atmos. Meas. Tech.*, vol. 10, no. 12, pp. 5039–5062, 2017, doi: 10.5194/amt-10-5039-2017.

[36] Y.-H. Cheng and M.-H. Lin, "Real-Time Performance of the microAeth® AE51 and the Effects of Aerosol Loading on Its Measurement Results at a Traffic Site," *Aerosol Air Qual. Res.*, vol. 13, pp. 1853–1863, 2013, doi: 10.4209/aaqr.2012.12.0371.

[37] G. S. W. Hagler, T. L. B. Yelverton, R. Vedantham, A. D. A. Hansen, and J. R. Turner, "Post-processing method to reduce noise while preserving high time resolution in aethalometer real-time black carbon data," *Aerosol Air Qual. Res.*, vol. 11, no. 5, pp. 539–546, 2011, doi: 10.4209/aaqr.2011.05.0055.

TABLES

Table 1 - Characteristics of 50m averaged *eBC* and *NP* profiles recorder in Adventalern. Median concentrations are compared with median values of maximum concentrations (MMC) and MMC height and *eBC* concentration in Longyearbyen (LYB, from AE33). These are calculated for the period of two hours before the sounding to the time of tethered balloon launch with eBC sensor in Adventdalen. *zTb* is the height of the temperature inversion.

Group profiles	Number		Median concentration		MMC		MMC height		LYB Median *eBC*, ng·m^{-3}
	eBC	*NP*	*eBC, ng·m^{-3}*	*NP, cm^{-3}*	*eBC, ng·m^{-3}*	*NP, cm^{-3}*	*eBC m*	*NP m*	
No temp inversion	43	32	94	**483**	**147**	**644**	350	**100**	**158**
zTb<500m	25	16	94	**1745**	**210**	**3080**	100	**0**	**181**
zTb>=500m	6	0	110	-	**194**	-	550	-	**199**

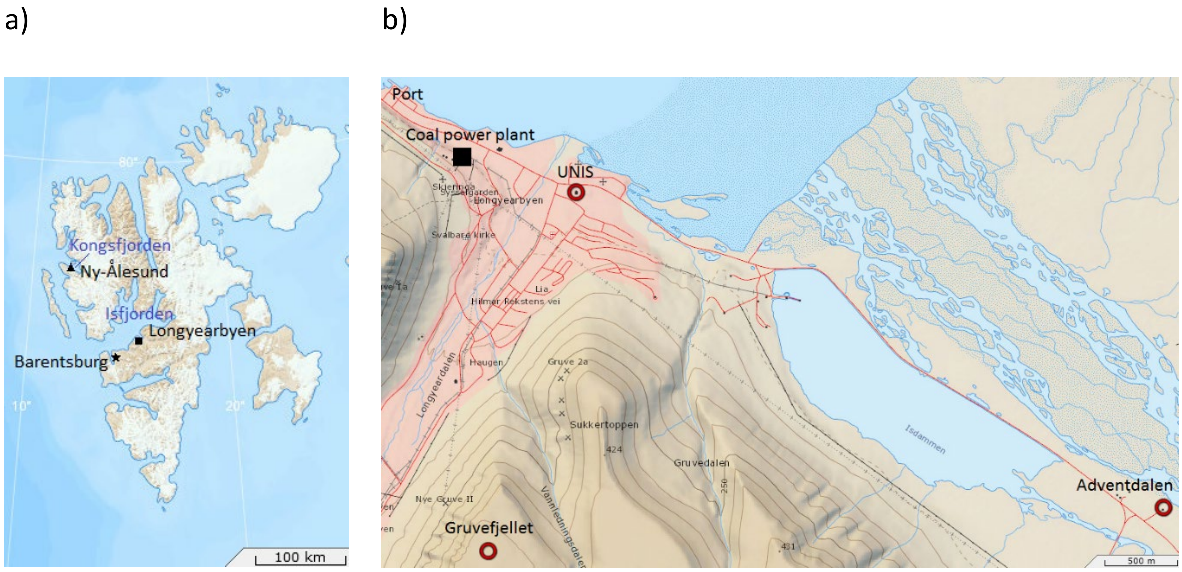

Figure 1. a) Map of Svalbard; b) local map of Longyearbyen

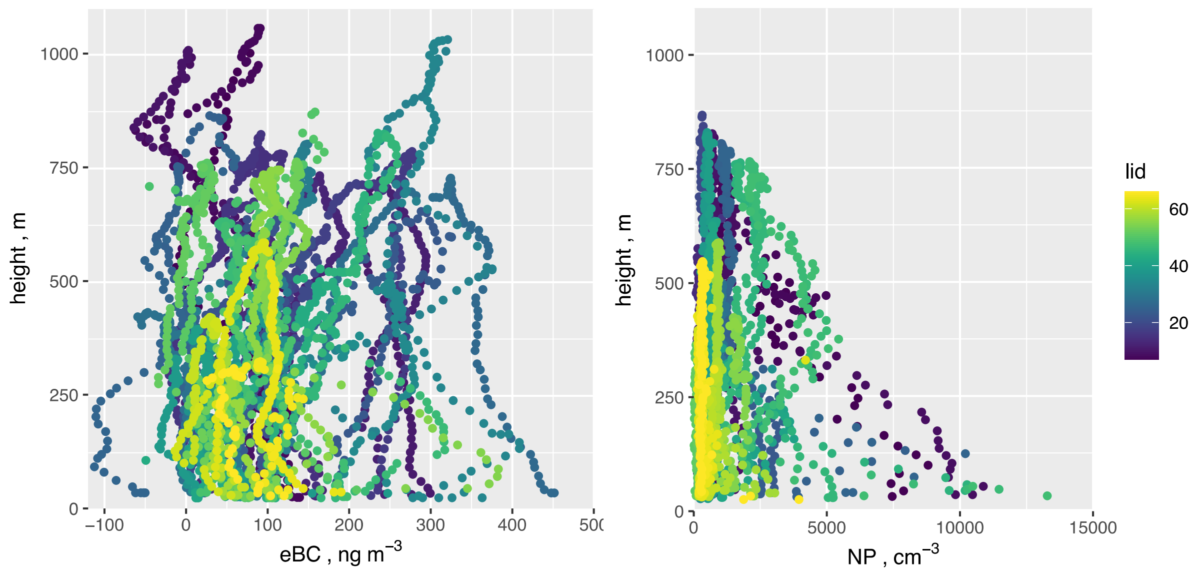

Figure 2 – Ungridded vertical profiles of (a) *eBC* and (b) *NP*. The color scale identifies the launch id (lid).

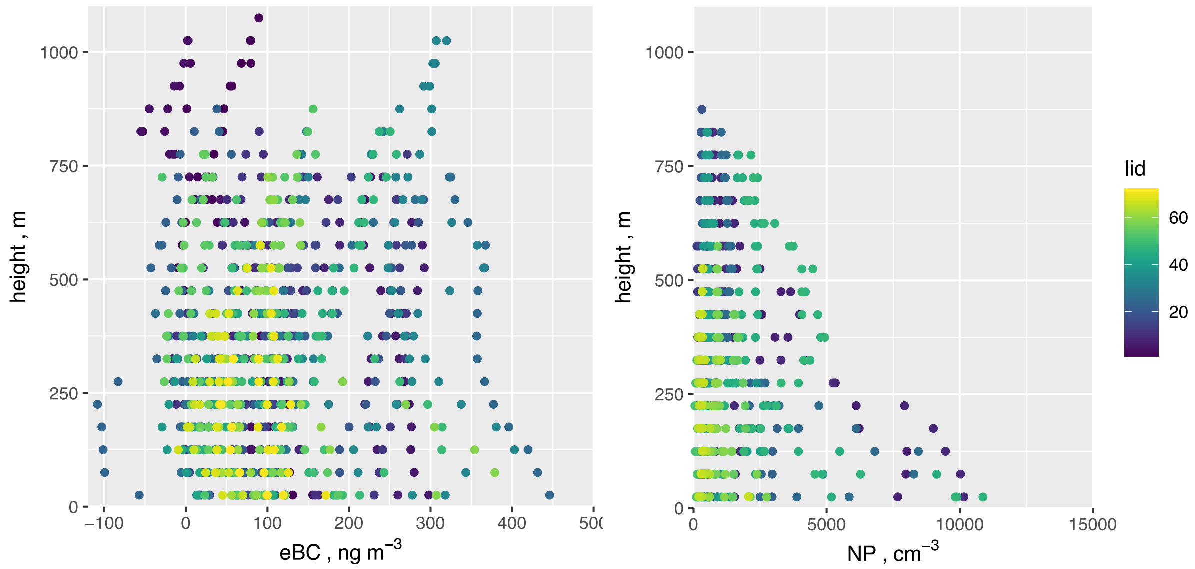

Figure 3 – Gridded vertical profiles of (a) *eBC* and (b) *NP*. The color scale identifies the launch id (lid).

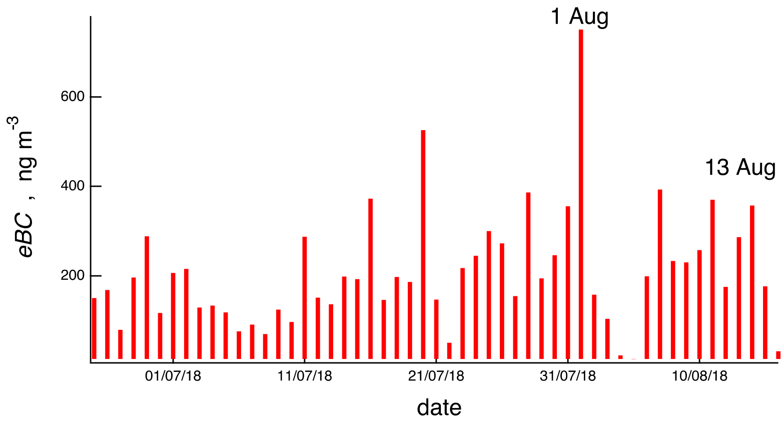

Figure 4 – Daily average eBC registered in LYB by the AE33.

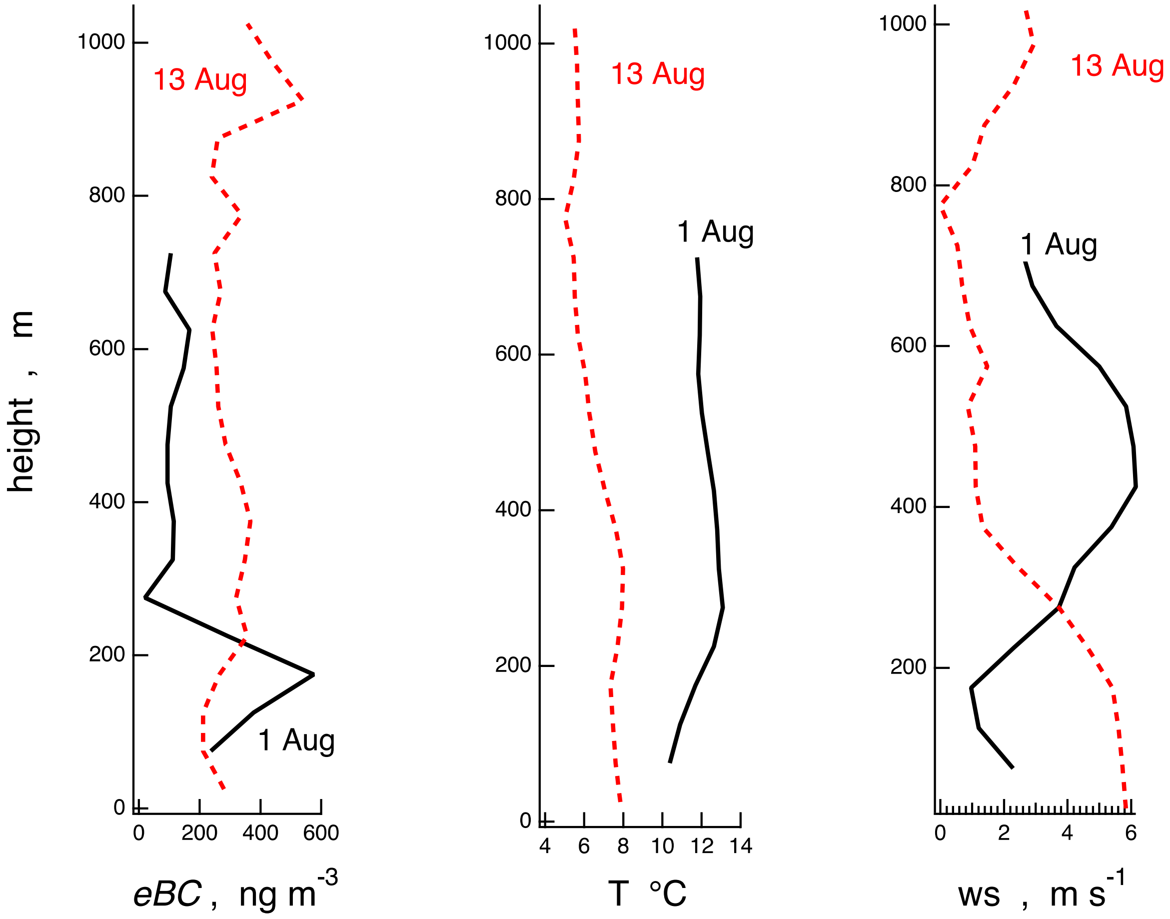

Figure 5 – Vertical profiles of eBC, temperature and RH registered with the tethered balloon system on the 1st of August (black continuous lines) and on the 13th of August (red dashed lines).

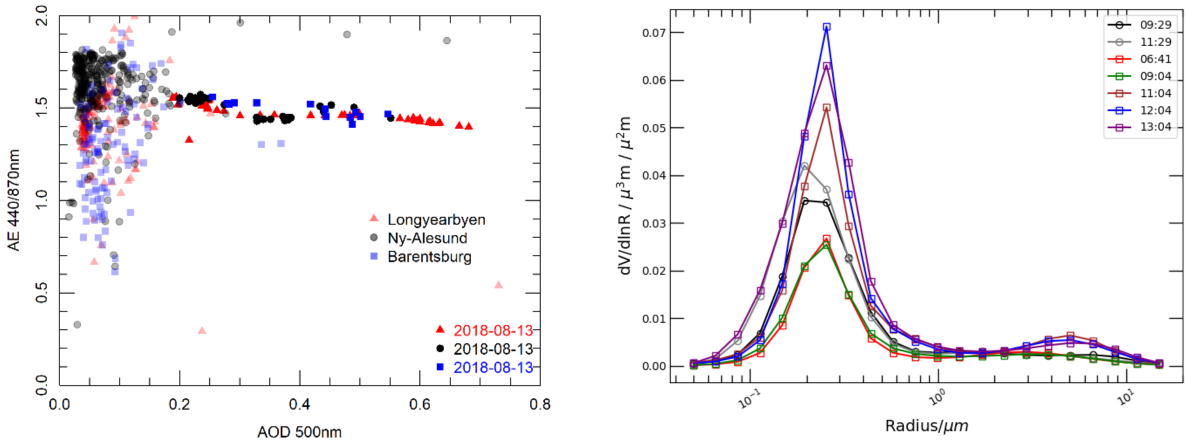

Figure 6 - a) Angstrom Exponent 440/870 nm as a function of the AOD at 500 nm; b) size distribution inversions for August 13th for Longyearbyen and Ny-Ålesund

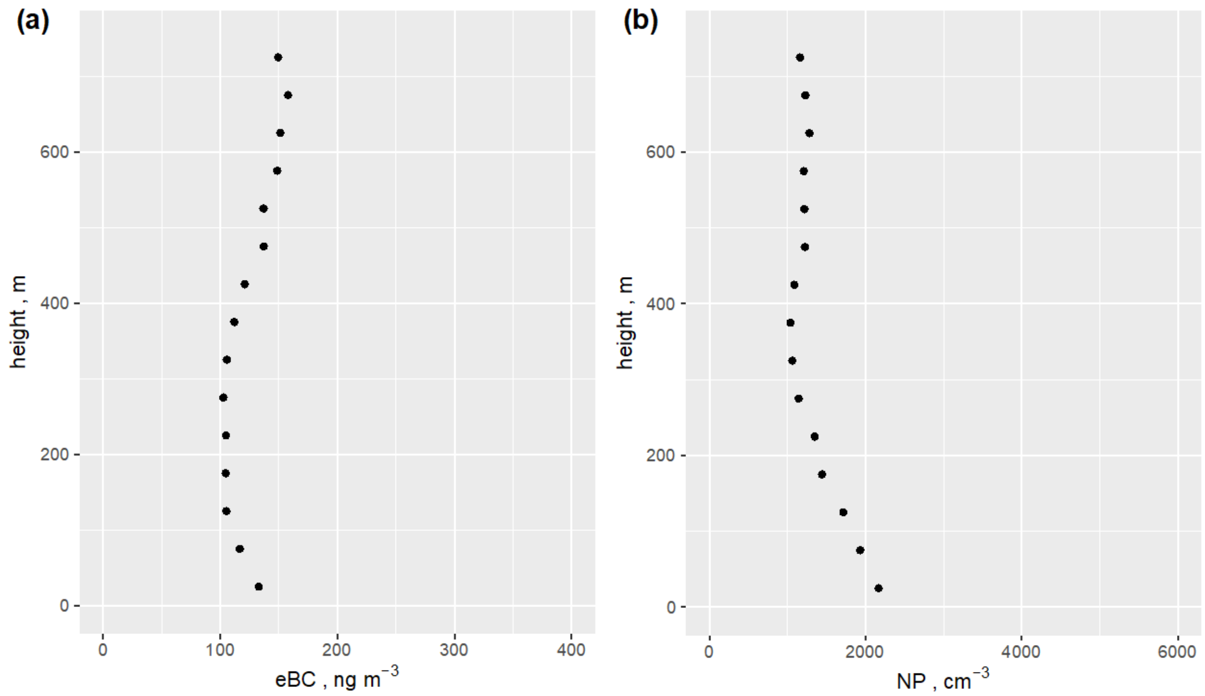

Figure 7 – Summertime averaged *eBC* and *NP* profiles along the atmospheric column over Longyearbyen in 2018. Shaded areas represent one SD of the population.

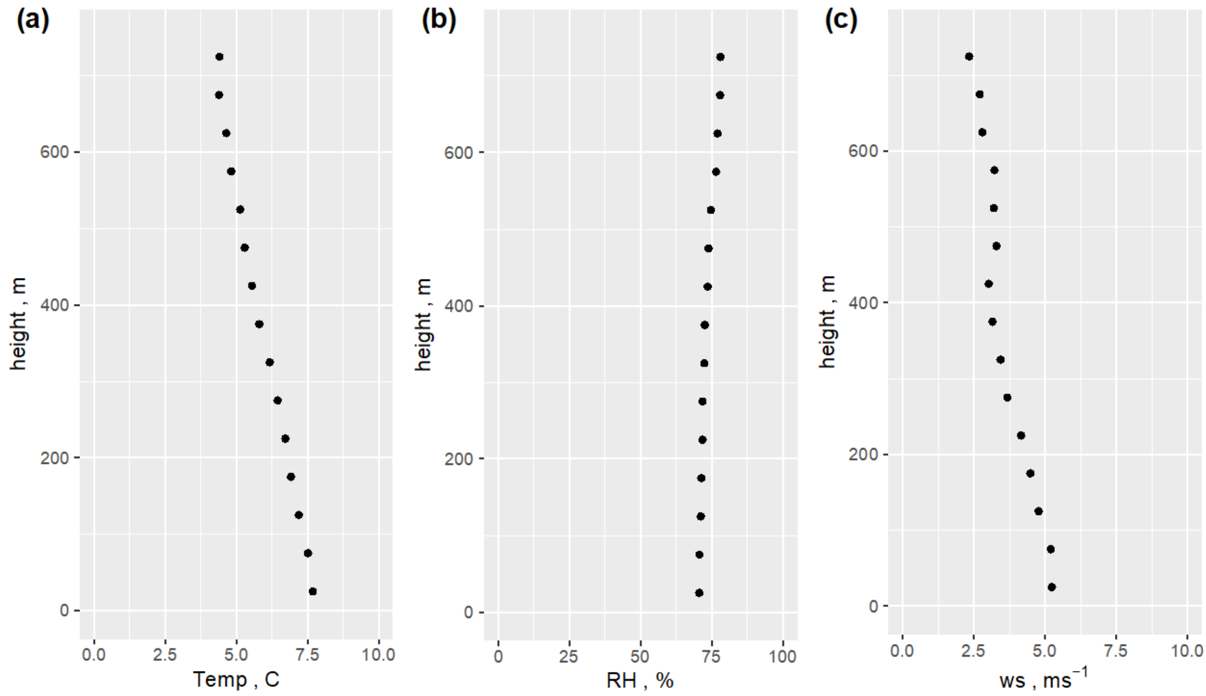

Figure 8 – Summertime averaged *T, RH* and wind speed (*ws*) profiles along the atmospheric column over Longyearbyen in 2018. Shaded areas represent one SD of the population

SUPPLEMENTARY MATERIAL FOR THE PAPER

Vertical profiles of black carbon and nanoparticles pollutants measured by a tethered balloon in an urban settlement in the Arctic

David Cappelletti[a,i*] Chiara Petroselli[b], David Mateos[c], M. Herreras[c], Luca Ferrero[d], Asta Gregorič[e], Claudia Frangipani[a], Gianandrea La Porta[a], Michael Lonardi[f], Alena Dekhtyareva[g,h]

Index

1. Intercomparison between AE51 and AE33 aethalometers

The relationship between the eBC concentrations measured with the AE51 and AE33, and correlation coefficient is not linear. We have divided all the calibration AE33 and AE51 data into 4 groups of almost equal size (~300 values in each) according to calculated AE33 eBC concentration quartiles: eBC values below 143 ng· m^{-3}, from 143 ng· m^{-3} to 297 ng· m^{-3}, from 297 ng· m^{-3} to 610 ng· m^{-3} and above> 610 ng· m^{-3}. As high time resolution eBC data is often noisy, especially at lower concentrations [35], [36], post-processing ONA-algorithm for noise reduction suggested by [37] was implemented on 30-seconds AE51 data before 1-minute averaging. The noise for AE51 1-minute averaged original data and data processed using ONA-algorithm was calculated for each group using the formula suggested by [37] and relative deviation of AE51 data from AE33 data was calculated using equation [36]. One can see that the correlation between AE51 and AE33 data increases rapidly for the eBC concentrations exceeding a 4th quartiles' limit, while relative deviation is the lowest for the same group (Table SM1).

Table SM1 - Calibration results between AE51 and AE33

Concentration group	Noise AE51, ng/m^3	Noise AE51-ONA, ng/m^3	Relative deviation (A51 and AE33)	Relative deviation (AE51-ONA and AE33)	Pearson r (A51 and AE33)	Pearson r (A51-ONA and AE33)
BC<q25	90	45	0.9±3.5	1.25±4.34	0.29	0.27
q25<=BC<q50	132	96	0.27±0.74	0.3±0.69	0.38	0.36
q50<=BC<q75	174	169	0.1±0.49	0.06±0.49	0.33	0.33
BC>q75	401	375	-0.04±0.33	-0.05±0.33	0.78	0.77
Total	220	166	0.31±1.83	0.39±2.26	0.87	0.87

FIGURE SM1 - Weather conditions in LYR during the study period.

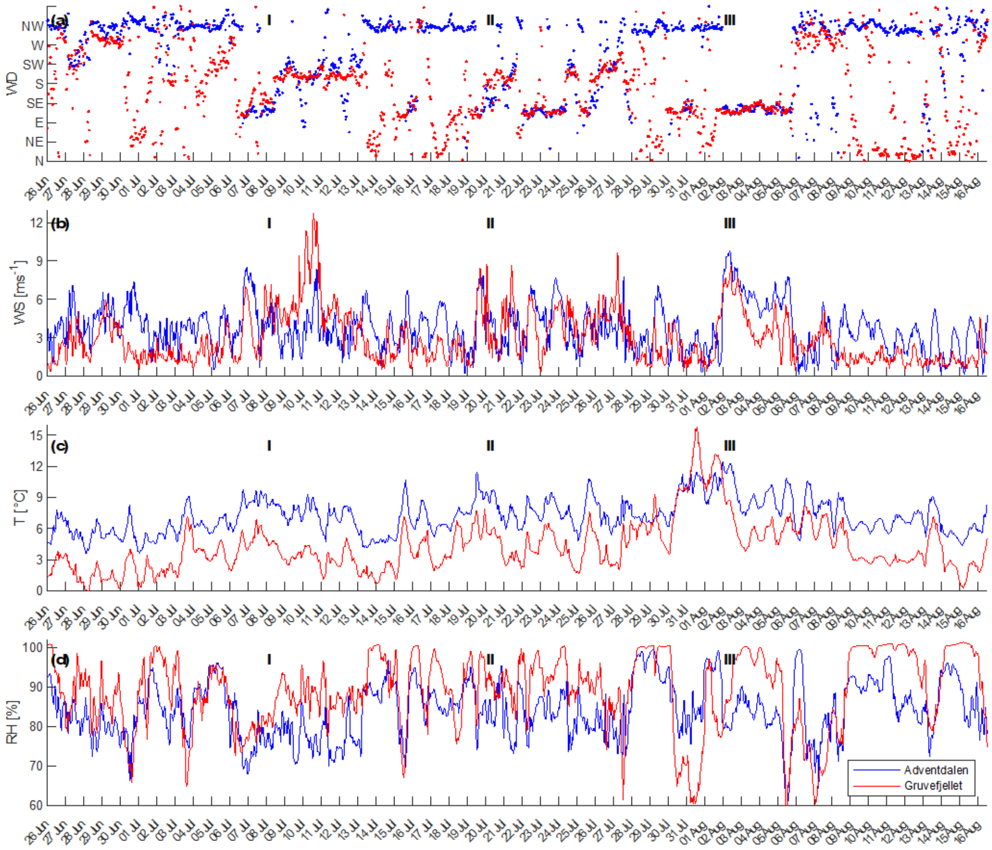

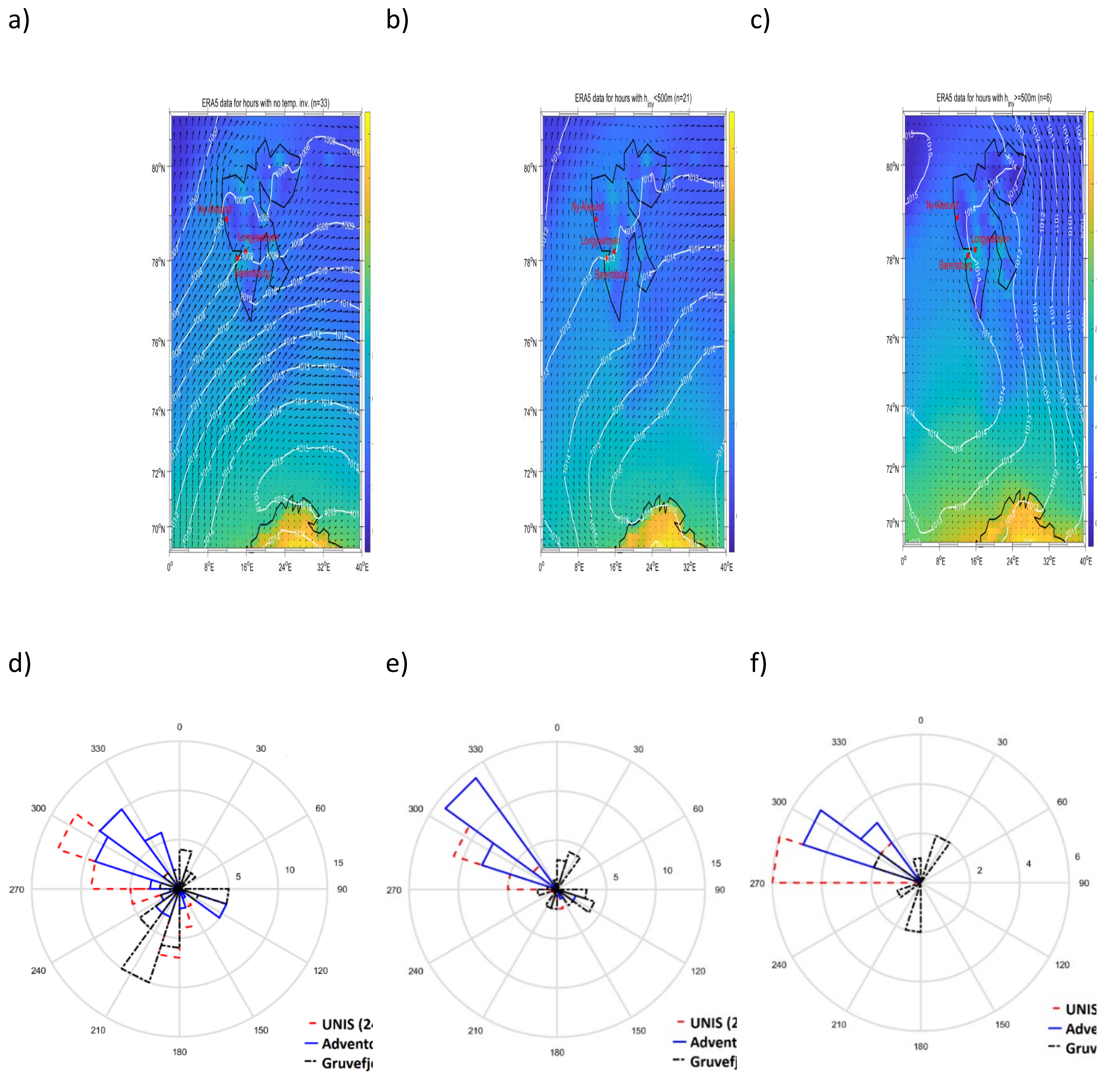

Figure SM2 a), b), c) Meteorological conditions for the three groups of Adventdalen profile data described in Table 1: mean air temperature in °C (colour scale), wind direction (black arrows) and mean sea-level pressure in hPa (white lines). (d), (e), (f) Wind measurements for the same three groups from Longyearbyen (UNI, 24 m a.s.l.), Adventdalen (Adv, 15 m a.s.l.) and Gruvefjellet (Gru, 464 m a.s.l.).

683

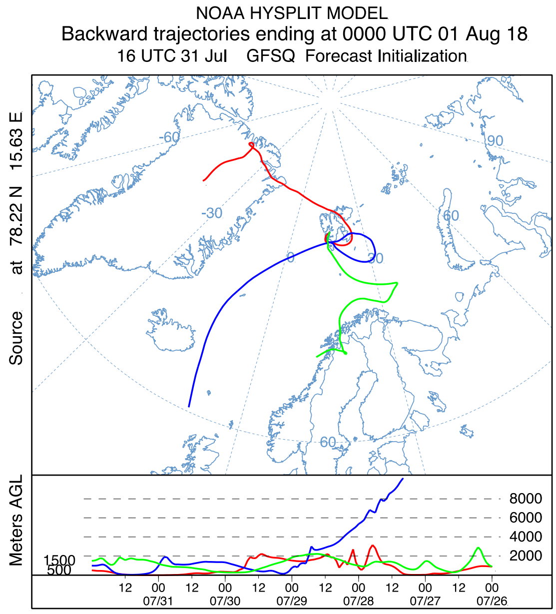

Figure SM3 – Air masses backward trajectories (HYSPLIT) arriving in LYB at 50, 500 and 1500 endpoints, the 1st of August at 00:00 UTC.

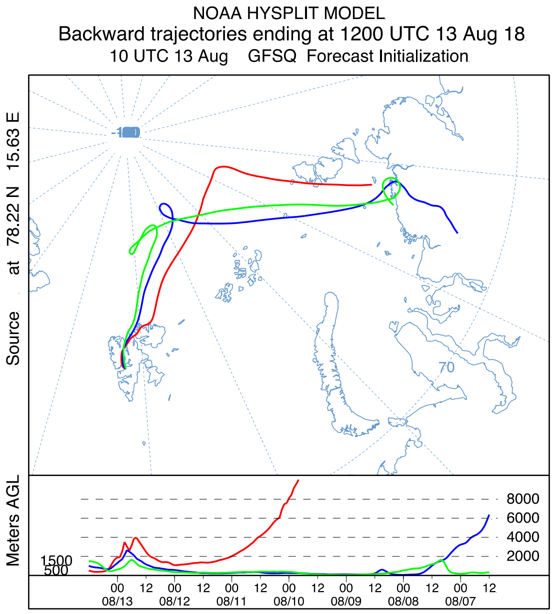

Figure SM4 – Air masses backward trajectories (HYSPLIT) arriving in LYB at 50, 500 and 1500 endpoints, the 13th of August at 12:00 UTC.